Understanding the morphotropic phase boundary of perovskite solid solutions as a frustrated state

Ying Shi Teh [1], Jiangyu Li,[2] and Kaushik Bhattacharya [1,*]

[1]*Division of Engineering and Applied Science, California Institute of Technology, Pasadena, California 91125, USA*

[2]*Department of Materials Science and Engineering, Southern University of Science and Technology, Shenzhen 518055, Guangdong, China*

(Received 18 December 2020; revised 7 March 2021; accepted 23 March 2021; published 5 April 2021)

This paper presents a lattice model incorporating random fields and long-range interactions where a frustrated state emerges at a specific composition but is suppressed elsewhere. The model is motivated by perovskite solid solutions and explains the phase diagram in such materials including the morphotropic phase boundary (MPB) that plays a critical role in applications for its enhanced dielectric, piezoelectric, and optical properties. Further, the model also suggests the possibility of phenomena by exploiting MPBs.

DOI: 10.1103/PhysRevB.103.144201

I. INTRODUCTION

Perovskites are materials with a chemical composition ABO_3, where A and B are typically transition metals that have a crystal structure similar to that of the mineral perovskite, $CaTiO_3$ ($Pm\bar{3}m$), Fig. 1(a) (e.g., Refs. [1,2]). Some of these materials undergo a displacive phase transition on cooling from the high temperature perovskite structure to a low temperature low symmetry structure that is not centrosymmetric and thus displays ferroelectricity or ferromagnetism. Therefore these materials are widely used in capacitor, ultrasonic, optical, sensor, and actuator applications for their dielectric and piezoelectric properties.

The basic structure is extremely stable, and it is possible to have solid solutions $A(C_xD_{1-x})O_3$ where two metallic species C and D substitutionally occupy the B site of the lattice. The low temperature structure in these compounds depends on composition and changes across the *morphotropic phase boundary* (MPB) which is largely independent of temperature. Figure 1(b) shows the phase diagram of the widely used piezoelectric lead zirconate titanate ($PbZr_xTi_{1-x}O_3$ or PZT) that has a MPB at $x = 0.52$ with a ferroelectric rhombohedral ($R3m$) structure in the Zr-rich compositions [1] and ferroelectric tetragonal ($P4mm$) structure in the Ti-rich compositions. The dielectric and piezoelectric properties as well as the ability to pole a ceramic increase dramatically at the MPB [3–5], and therefore PZT is widely used close to this composition. The search for lead-free dielectric and piezoelectric materials has also focused on solid solutions with MPBs (e.g., Ref. [6]).

The nature of the MPB has been extensively studied since the discovery of a bridging monoclinic phase (Cm) at the MPB by Noheda *et al.* [7] using x-ray powder diffraction. It has been suggested that the presence of a bridging phase enables a larger intrinsic [4,8,9] and extrinsic [5] piezoelectric effect at the MPB. Since then, various structures have been observed: the combination of two monoclinic phases (Cm and Ic [10] or Cm and Pm [11]), combination of tetragonal ($P4mm$) and monoclinic (Cm) [12], and combination of rhombohedral ($R3m$) and monoclinic (Cm) [13]. This uncertainty has been attributed to the disorder in the composition which further results in a disorder in the structure and the difficulty of resolving local structures [14]. This role of disorder is also supported by first principles calculations [15,16]. This, however, raises the question as to why the disorder does not affect the structure away from the MPB. Another interesting observation concerns the domain patterns. Classical well-defined domain patterns are observed away from the MPB, but highly fragmented domain patterns are observed near the MPB [17]. It has been argued that this fragmented domain pattern also contributes to the high piezoelectric response [18].

In short, critical questions remain open. Why is the effect of compositional disorder suppressed to form an unambiguous structure away from the MPB but suddenly revealed at the MPB? Is there a definitive crystal structure at the MPB? Why do domain patterns become fragmented near the MPB? Does compositional disorder play a role in the ease of poling at the MPB? Can the MPB be exploited to create new phenomena? These questions have proved to be challenging. The disordered nature of the solid solution requires a large ensemble that takes it beyond the scope of first principles calculations without the introduction of a composition-dependent hybrid pseudopotential [19] that does not include randomness. On the other hand, phase-field Landau-Ginzburg methods can provide insight into domain patterns but require a phenomenological model of the phase transition.

In this paper, we propose a model based on the random-field Ising model with long-range interactions that incorporates the basic elements of the underlying physics. The B sites of a perovskite form a reference cubic lattice that is occupied randomly by atoms of either C or D species. The local quantum mechanical interactions create a propensity for the unit cell to break cubic symmetry depending on the species at the B site. The ferroelectric, ferromagnetic, and ferroelastic polarizations lead to long-range interactions. We create an effective Hamiltonian with these physics.

*Corresponding author: bhatta@caltech.edu

[1]PZT shows a second rhombohedral ($R3c$) phase at low temperature at high Zr compositions, but we focus on the compositions near the MPB.

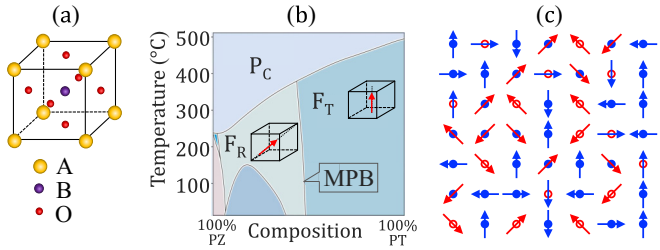

FIG. 1. (a) Perovskite structure. (b) Phase diagram of PZT adapted from Cross [3]. F_R, F_T, and P_C denote ferroelectric rhombohedral, tetragonal, and paraelectric phases, respectively. (c) Schematic illustration of the lattice model proposed in this work.

In the first part of the paper, we show that our model provides insights to the questions concerning the MPB of ferroelectric solid solutions like PZT. In particular, the long-range interactions overwhelm the local disorder in the C-rich and D-rich compositions with the exchange of stability taking place at a specific composition where the material is frustrated. This frustration manifests itself as the MPB. The frustrated state also enables easy poling as observed. In the second part, we use the model to explore the possibility of obtaining a strongly coupled multiferroic material system using the insights obtained from the first part.

II. MPB IN FERROELECTRIC MATERIALS

A. Model

Consider a d-dimensional periodic lattice ($d = 2$ or 3) with N lattice points as shown in Fig. 1(c). Each lattice point i is characterized by fixed (quenched) chemical composition (c_i) of either type C [$c_i = 0$ indicated by a red open circle in Fig. 1(c)] or type D [$c_i = 1$ indicated by a blue closed circle]. Each lattice point carries a dipole state [$\boldsymbol{p}_i$ indicated by the arrows in Fig. 1(c)] that can take one of a number of orientations $\mathcal{C} \cup \mathcal{D}$ determined by the Hamiltonian

$$W(\{\boldsymbol{p}_i\};\{c_i\}) = \sum_{i=1}^{N} h_i - \frac{1}{2}\sum_{<i,j>} J_{e_{ij}} \boldsymbol{p}_i \cdot \boldsymbol{p}_j + W_e. \quad (1)$$

The first term encodes the information that lattice site of type C (respectively, D) energetically prefers the set of dipole states $\mathcal{C}$ indicated by the red arrows (respectively, $\mathcal{D}$ indicated by the blue arrows), though they can take states in $\mathcal{D}$ (respectively, $\mathcal{C}$) with an energetic cost $h_{C\mathcal{D}} > 0$ (respectively, $h_{D\mathcal{C}} > 0$):

$$h_i = \begin{cases} h_{C\mathcal{D}} & c_i = 0 \;\&\; \boldsymbol{p}_i \in \mathcal{D}, \\ h_{D\mathcal{C}} & c_i = 1 \;\&\; \boldsymbol{p}_i \in \mathcal{C}, \\ 0 & \text{otherwise.} \end{cases} \quad (2)$$

The second term, where the sum is limited to nearest neighbors, is the exchange energy. Ferroelectricity requires noncentrosymmetric displacements of ions which arise from a delicate balance between short-range repulsions of electron clouds and a short-range portion of the Coulomb interaction with a range of the lattice constant [20]. The exchange term captures this net ferroelectric effect as it promotes like neighbors when the exchange constant $J_{e_{ij}} > 0$. The exchange constant in this model is composition dependent and takes the form of

$$J_{e_{ij}} = \frac{1}{2}[J_e(c_i) + J_e(c_j)], \quad J_e(c) = \begin{cases} J_e^C & c = 0, \\ J_e^D & c = 1. \end{cases} \quad (3)$$

The third term represents the electrostatic contribution that includes the long-range dipole-dipole interaction scaled by D_e (which incorporates the dipole strength, lattice constant, and electromagnetic constants) and the influence of the applied external electric field $\boldsymbol{E}$.

$$\begin{aligned} W_e &= W_{em}(\{\boldsymbol{p}_i\}, D_e, \boldsymbol{E}) \\ &:= D_e\left(\frac{1}{(d-1)}\sum_{i,j=1}^{N}{\sum_{\mathbf{R}}}' \frac{1}{r_{ij}^d}\left[\boldsymbol{p}_i \cdot \boldsymbol{p}_j - \frac{d(\boldsymbol{p}_i \cdot \mathbf{r}_{ij})(\boldsymbol{p}_j \cdot \mathbf{r}_{ij})}{r_{ij}^2}\right]\right. \\ &\quad \left. + \frac{2\pi}{d}\sum_{i=1}^{N}|\boldsymbol{p}_i|^2\right) - \boldsymbol{E} \cdot \sum_{i}^{N} \boldsymbol{p}_i. \end{aligned} \quad (4)$$

Given a lattice where the composition of each site is randomly assigned subject to a fixed average, we use a Markov chain Monte-Carlo (MCMC) method with cooling to obtain the equilibrium distribution at a given temperature. The state is initialized by randomly assigning a polarization from $\mathcal{C} \cup \mathcal{D}$. Adapting the Metropolis-Hastings algorithm to our multistate setting, a site is chosen at random and its dipole state is updated to one of the N_s states according to the transition probability

$$P_s = \frac{\exp(-\beta W^{(s)})}{\sum_{r=1}^{N_s}\exp(-\beta W^{(r)})}, \quad s = 1, ..., N_s, \quad (5)$$

where β is the inverse temperature and N_s is the cardinality of $\mathcal{C} \cup \mathcal{D}$. We avoid the system getting trapped in local minima at low temperatures by starting at a high temperature ($\beta = 0$) and slowly cooling (increasing β) to the temperature of interest, while performing enough MCMC steps to reach equilibrium at each temperature.

Note that the dipole-dipole term is conditionally convergent. So, we adopt Ewald summation [21–23] to separate it into a short-range contribution that converges rapidly in real space, a long-range contribution that converges rapidly in Fourier space, a self energy, and a surface term that depends on the boundary condition. Further, notice that for any flip, $\Delta W_e \approx -\boldsymbol{E}_i \cdot \Delta \boldsymbol{p}_i$ where $\boldsymbol{E}_i = -\nabla_{\boldsymbol{p}_i} W_e$ is the electric field. While $\boldsymbol{E}_i$ has to be recomputed after each flip, the error is small for individual flips. Therefore we update $\boldsymbol{E}_i$ only every $\sqrt{N}$ flips where N is the size of the lattice. We can then perform $\sqrt{N}$ flips independently and in parallel thereby enabling acceleration on a graphical processing unit (GPU). Further, $\boldsymbol{E}_i$ is readily computed using fast Fourier transforms which can also be implemented on GPUs. Further details are provided in Supplemental Material [24].

B. Results

We study an example motivated by PZT though the results are generic. Here, the C and D lattice points represent lead zirconate (PZ) and lead titanate (PT) unit cells containing Zr and Ti atoms, respectively. Recall that the former prefers rhombohedral or ⟨111⟩ polarization states while the latter prefers tetragonal or ⟨100⟩

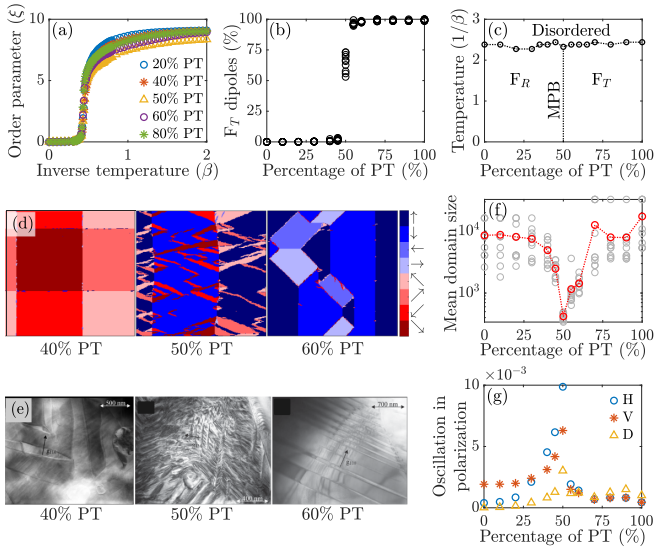

FIG. 2. Emergence of a morphotropic phase transition (MPB) as a competition between short-range (compositional) disorder and long-range (exchange and electrostatic) interactions. (a) Order parameter vs inverse temperature for various compositions. (b) Dipole orientation in the ordered phase at various compositions. (c) Phase diagram showing the MPB. (d) Domain patterns at various composition. (e) Experimentally observed domain patterns at various compositions (reprinted with permission from Woodward, Knudsen, and Reaney [17]). (f) Average domain size vs composition [average (red) and ten realizations (gray)]. (g) Small-scale oscillations in terms of the finest Haar wavelet horizontal (H), vertical (V), and diagonal (D) detail coefficients vs composition.

polarization states. We consider two dimensions $d = 2$ so that $\mathcal{C} = (p_o^{\mathcal{C}}/\sqrt{2})\{[1, 1], [1, -1], [-1, 1], [-1, -1]\}$ while $\mathcal{D} = p_o^{\mathcal{D}}\{[1, 0], [0, 1], [-1, 0], [0, -1]\}$. Unless otherwise specified, we set $p_0^{\mathcal{C}} = p_0^{\mathcal{D}} = h_{\mathcal{CD}} = h_{\mathcal{DC}} = J_e^C = J_e^D = D_e = 1$, unit lattice distance between any two nearest neighboring sites, and conduct our simulations on a 256^2 lattice. The lattice size is chosen to be sufficiently large upon convergence studies [24] to depict randomness in composition as well as for us to visualize domain formation. In each simulation, we begin with an inverse temperature of $\beta = 0$ and repeatedly increase its value with a small step size of $\Delta\beta = 0.05$ until we reach $\beta = 5$. At each temperature value, at least 2000 Monte Carlo (MC) sweeps (each sweep consists of $N = 256^2$ steps) are performed with a total of approximately 2×10^5 sweeps.

Figure 2 shows the results of these simulations. Figure 2(a) shows the evolution of the order parameter [$\xi = \frac{1}{\kappa_{\max}} \sum_{\kappa=1}^{\kappa_{\max}} \kappa C(\kappa)$, where $C(\kappa) = \langle \boldsymbol{p}_i \cdot \boldsymbol{p}_j \rangle$ is the correlation function over any two sites i and j that satisfy $\kappa - 1 < |\mathbf{r}_i - \mathbf{r}_j| \leqslant \kappa$] in a series of simulations with varying average composition. The material is disordered at high temperature but becomes ordered at low temperatures. The phase transition is somewhat diffuse due to the compositional disorder. Figure 2(b) shows the nature of the ordered phase. Remarkably, we find that all dipoles are in the rhombohedral ($\mathcal{C}$) states until a critical composition of about 50% beyond which all dipoles are in the tetragonal ($\mathcal{D}$) states. Indeed, at a composition of 33.3%, a third of the sites would prefer tetragonal dipoles. However, the exchange and electrostatic interaction with the neighbors overwhelm this preference and instead force it into the rhombohedral state. The opposite happens at a composition of 66.7%. The exchange of stability between the rhombohedral and tetragonal states takes place at a well-defined critical composition. This observation is extremely robust: Figure 2(b) includes results from 10 realizations. In short, we see the *emergence of the morphotropic phase boundary* (MPB). Remarkably, the disorder is completely suppressed at all compositions except the MPB.

The resulting phase diagram is shown in Fig. 2(c) (where the order-disorder transition temperature is taken to be that of the maximum curvature of the $\xi - \beta$ curve). It is structurally consistent with experimental observations with the paraelectric phase at high temperature and different ordered phase at low temperatures depending on composition. The details depend on the parameters as we shall show later.

The resulting domain patterns are also interesting. Figure 2(d) shows the typical domain patterns at three different compositions (Animations of the simulations are provided in Ref. [24]). We see the 2D analogs of 71° or 109° domain walls with (10) normals at composition of 40%, and we see the 2D analog of 90° domain walls with (11) normals at composition of 60%. However, at the MPB (composition 50%), we see a mixture of rhombohedral ($\mathcal{C}$) and tetragonal ($\mathcal{D}$) states with a highly fragmented and frustrated domain pattern. Figure 2(f) shows that the average domain size falls precipitously at the MPB compared to that at all other compositions. Figure 2(g) shows that the oscillations in polarization in the horizontal, vertical, and diagonal directions are also magnified at the MPB. Specifically, we take the Haar wavelet transform of the domain pattern, and Fig. 2(g) shows the normalized sum of squares of the horizontal, vertical, and diagonal detail coefficients obtained from level one (finest level) Haar wavelet decomposition averaged over 10 realizations. All these observations are consistent with experimental observations. Figure 2(e) reproduces the experimental observations of Woodward, Knudsen, and Reaney [17]: classical well-defined domain patterns are observed away from the MPB, but highly fragmented domain patterns are observed near the MPB as in our simulations [Fig. 2(d)]. We note that the fragmented patterns in our simulations at the MPB are found to be angled at around 22.5° to accommodate divergence-free rotation of dipole states across the boundary when changing from a tetragonal state to a rhombohedral state or vice versa. Such domain walls typically do not exist in three dimensions leading to further fragmentation [25].

We comment that both the long-range interaction and the disorder in composition are necessary for this behavior. In the absence of the long-range dipole-dipole interaction (i.e., when $D_e = 0$), the average number of dipoles track the composition as shown in Fig. 3(a). The lower critical dimension of a two-state random field Ising model is two, i.e., the lattice remains disordered even at low temperatures [26,27]. This is consistent with the observations in the first row of Fig. 3(b) where the material remains disordered. We see some domains, with $\mathcal{C}$-rich states and $\mathcal{D}$-rich states and meandering domain walls. However, the microstructure is still disordered with all states present, and domains with $\mathcal{C}$-rich and $\mathcal{D}$-rich states coexist. This is why the average number of dipoles track the composition. Crystallographically distinguished domain walls arise

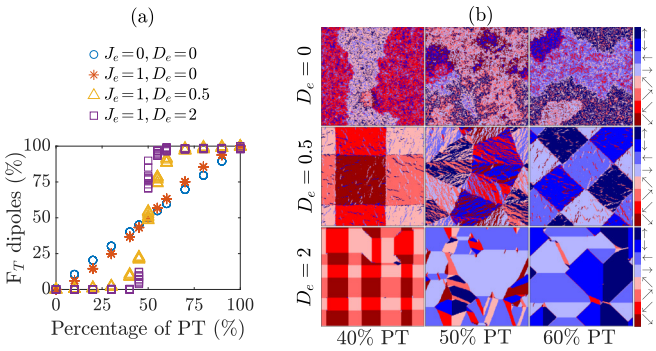

FIG. 3. The effect of different dipole-dipole interaction strength D_e. (a) and (b) show the dipole orientation and domain patterns in the ordered phase at various compositions and D_e values. $J_e = 1$ in (b).

with small D_e and become sharper as it increases [Fig. 3(b)] along with a complete suppression of the disorder within the domains. Finally, at large D_e, we see less fragmented domains at the MPB because the role of disorder becomes comparably smaller. The complex domain patterns at the MPB also do not appear when the composition is not random [24].

Figure 4 shows how the phase diagram changes as we change the relative magnitudes of $h_{\mathcal{CD}}$, $h_{\mathcal{DC}}$ and $J_e^{\mathcal{C}}$, $J_e^{\mathcal{D}}$ while keeping their averages the same. The columns show that the order-disorder transformation temperature becomes composition dependent when $J_e^{\mathcal{C}} \neq J_e^{\mathcal{D}}$ with the slope of the transition temperature dependent on the relative magnitudes of $J_e^{\mathcal{C}}$ and $J_e^{\mathcal{D}}$ while the rows show that the MPB composition depends critically on the relative magnitude of $h_{\mathcal{CD}}$ and $h_{\mathcal{DC}}$. Figure 5 shows that the MPB composition also depends sensitively on the relative polarization magnitudes $p_0^{\mathcal{C}}$ and $p_0^{\mathcal{D}}$.

An explicit solution of this problem remains open, but we can understand various aspects qualitatively. We first consider the order-disorder phase transition temperature T_c. Recall that according to the Onsager solution to the (two state) Ising

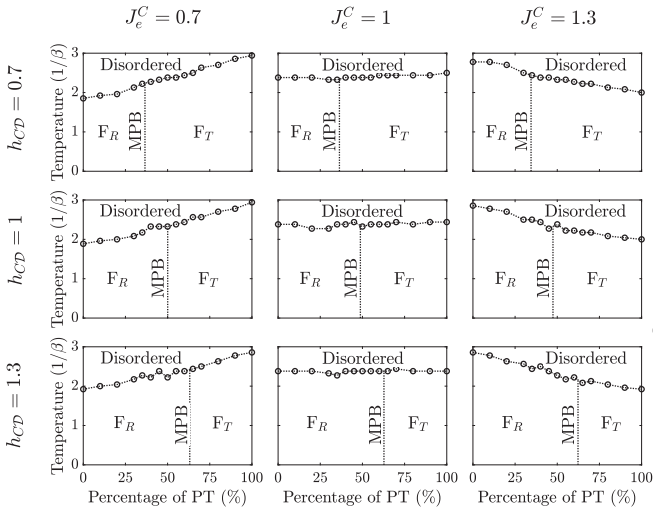

FIG. 4. The effect of different energetic penalties and exchange constants for different composition types of phase diagram. $h_{\mathcal{CD}}$ and $J_e^{\mathcal{C}}$ are varied with both $(h_{\mathcal{CD}} + h_{\mathcal{DC}})/2$ and $(J_e^{\mathcal{C}} + J_e^{\mathcal{D}})/2$ kept constant at 1.

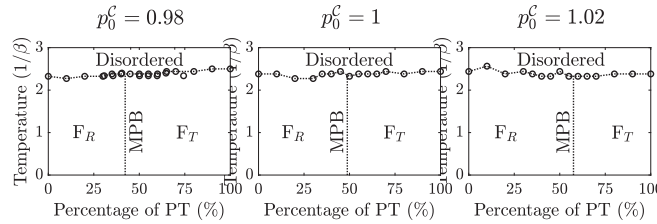

FIG. 5. The effects of dipole magnitude $(p_0^{\mathcal{C}}, p_0^{\mathcal{D}})$. $p_0^{\mathcal{C}}$ is varied with $(p_0^{\mathcal{C}} + p_0^{\mathcal{D}})/2$ kept constant at 1.

model on a square lattice, $T_c = 2J_e/\ln(1+\sqrt{2}) = 2.27$ for $J_e = 1$. At the two pure end states, there is no disorder, but we differ from the Ising model in two important ways. First, we have eight allowable states and we expect this to depress T_c. Second, we have dipole-dipole interactions; the energy due to this is high in the disordered state but is driven to almost zero by the formation of domains in the ordered states. Consequently we expect the T_c to increase with D_e. We have confirmed this: For $J_e = 1$, we find T_c to be 1.3, 2.0, 2.3, 2.9 for $D_e = 0, 0.5, 1, 2$, respectively, for the end states. In any case, for D_e fixed, we expect T_c to be proportional to J_e as we see in Fig. 4 for the end states. In fact, this is also true in the intermediate compositions since the disorder in chemical composition has little effect on T_c. The average J_e is $(1-\lambda)J_e^{\mathcal{C}} + \lambda J_e^{\mathcal{D}}$ for a disordered lattice with volume fraction λ of D sites. Consequently we expect T_c to be proportional to λ as we see in Fig. 4.

We now turn to the MPB composition λ_c. We consider very low temperature where the entropy can be neglected. Since the dipole-dipole energy suppresses the disorder, we simply need to compare the energy between the configuration where every lattice point is in a $\mathcal{C}$ state with one where every lattice point is in a $\mathcal{D}$ state. Further, the formation of domains can reduce the dipole-dipole energy. Therefore, to leading order, the energy in these configurations is

$$W^{\mathcal{C}} = \lambda h_{\mathcal{DC}} - 2\left[(1-\lambda)J_e^{\mathcal{C}} + \lambda J_e^{\mathcal{D}}\right]\left(p_0^{\mathcal{C}}\right)^2,$$
$$W^{\mathcal{D}} = (1-\lambda)h_{\mathcal{CD}} - 2\left[(1-\lambda)J_e^{\mathcal{C}} + \lambda J_e^{\mathcal{D}}\right]\left(p_0^{\mathcal{D}}\right)^2. \quad (6)$$

Equating the two, we obtain

$$\lambda_c = \frac{h_{\mathcal{CD}} + 2J_e^{\mathcal{C}}\left[\left(p_0^{\mathcal{C}}\right)^2 - \left(p_0^{\mathcal{D}}\right)^2\right]}{h_{\mathcal{CD}} + h_{\mathcal{DC}} + 2\left(J_e^{\mathcal{C}} - J_e^{\mathcal{D}}\right)\left[\left(p_0^{\mathcal{C}}\right)^2 - \left(p_0^{\mathcal{D}}\right)^2\right]}. \quad (7)$$

This is consistent with the results in Fig. 4 [e.g., in the middle column where $J_e^{\mathcal{C}} = J_e^{\mathcal{D}} = p_0^{\mathcal{C}} = p_0^{\mathcal{D}} = 1$, $\lambda_c = h_{\mathcal{CD}}/(h_{\mathcal{CD}} + h_{\mathcal{DC}}) = h_{\mathcal{CD}}/2$, which is 0.35, 0.5, 0.65 in the three rows] and Fig. 5 [$h_{\mathcal{CD}} = h_{\mathcal{DC}} = J_e^{\mathcal{C}} = J_e^{\mathcal{D}} = 1$, so $\lambda_c = 1/2 + 2(p_0^{\mathcal{C}} - p_0^{\mathcal{D}})$ which is 0.42, 1, 0.58 in the three cases].

The situation is largely similar with some difference in detail in three dimensions (see Ref. [24]). We observe that the MPB emerges with local and exchange energies even in the absence of long-range dipole-dipole interactions ($D_e = 0$). This is consistent with the fact that local critical dimension of a random-field Ising model is two. In a random-field Ising model with two states and positive exchange constant, the lattice is disordered in two dimensions (i.e., does not undergo the order-disorder transition) while the lattice can be ordered

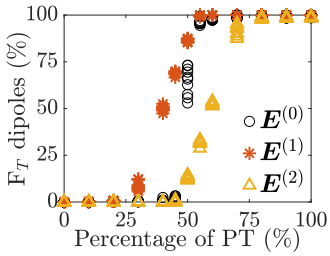

FIG. 6. The effects of external electric field ($\boldsymbol{E}^{(0)} = [0\ 0], \boldsymbol{E}^{(1)} = [6\ 0], \boldsymbol{E}^{(2)} = [\frac{6}{\sqrt{2}}\ \frac{6}{\sqrt{2}}]$). There is superior ability to pole at the MPB.

in three dimensions under a small random field at sufficiently low temperature [26,27]. However, the domain patterns look more like those shown in the first row of Fig. 3(b) than actual ferroelectric domains in the absence of long-range interactions. Our results are also consistent with the observation that dipolar interactions in an Ising model with two states leads to stripe domains in two dimensions [28].

Finally, we consider the effect of an applied external electric field in Fig. 6. Under [1 0] field that makes the tetragonal ($\mathcal{D}$) dipoles energetically more favorable, we still see that the tetragonal dipoles continue to be suppressed for small Ti (D) concentrations. However, tetragonal dipoles emerge gradually at a composition smaller than the MPB, increasing with composition until they become all tetragonal at a composition slightly larger than the MPB. So, there is a transition with composition, but transition is gradual and not sharp as in the case of zero electric field. There is a corresponding behavior when an electric field is applied in the [1 1] direction. This shows that materials close to the MPB can undergo an electric-field-imposed rhombohedral/tetragonal transition close to the MPB but not at other compositions. This is consistent with experimental observations [29]. The corresponding microstructures are shown in Ref. [24].

III. MULTIFERROIC MATERIALS

We now seek to apply the insights offered by the model to explore new phenomena. A number of perovskites are known to be ferromagnetic [30]. We explore the possibility of creating a multiferroic material (one that shows a strong coupling between electric and magnetic polarization) by exploiting the insight that the competition between short-range disorder and long-range interaction can lead to unique ordering behavior. Such multiferroic coupling is limited in single materials [31] and typically realized using composite media.

Consider a solid solution of two materials, C which prefers the $\mathcal{C}$ states that are ferroelectrically polarized in one crystallographic direction but with no ferromagnetism, and a material D that prefers the $\mathcal{D}$ states that are ferromagnetically polarized in a different crystallographic direction but with no ferroelectricity. The states are also mechanically distorted with the spontaneous strain corresponding to their ferroelectric/ferromagnetic directions. Since perovskites readily form solid solutions, and since perovskites can be both ferroelectric and ferromagnetic, it is natural to look for such systems in this class of materials.

A. Model

As before, consider a d-dimensional periodic lattice ($d = 2$ or 3) with N lattice points where each lattice point has a fixed (quenched) chemical composition ($c_i \in \{0, 1\}$ representing materials C or D, respectively). The state s_i at the ith lattice point is characterized by an electrical dipole $\boldsymbol{p}_i$, magnetic dipole $\boldsymbol{m}_i$ and an elastic strain $\boldsymbol{e}_i$, and governed by the Hamiltonian

$$W(\{s_i\};\{c_i\}) = \sum_{i=1}^{N} h_i - \frac{J_e}{2}\sum_{<i,j>} \boldsymbol{p}_i \cdot \boldsymbol{p}_j - \frac{J_m}{2}\sum_{<i,j>} \boldsymbol{m}_i \cdot \boldsymbol{m}_j + W_e + W_m + W_s, \quad (8)$$

where

$$h_i = \begin{cases} 0 & c_i = 0\ \&\ s_i \in \mathcal{C},\ \text{or, } c_i = 1\ \&\ s_i \in \mathcal{D} \\ h & \text{otherwise} \end{cases} \quad (9)$$

describes the local preference, W_e is the electrostatic interaction as in (4), W_m is the magnetostatic interaction under an applied magnetic field $\boldsymbol{H}$ ($W_m = W_{em}(\{\boldsymbol{m}_i\}, D_m, \boldsymbol{H})$), and W_s is the strain energy. The strain energy is that of a continuum region with transformation strain $\boldsymbol{e}^*(\mathbf{r})$ and uniform isotropic elastic modulus. For simplicity, it is scaled by parameter D_s to include these material constants. We set $\boldsymbol{e}^*(\mathbf{r}) = \begin{bmatrix} e_1^*(\mathbf{r}) & e_2^*(\mathbf{r}) \\ e_2^*(\mathbf{r}) & -e_1^*(\mathbf{r}) \end{bmatrix}$ and assume that $\boldsymbol{e}^*(\mathbf{r})$ is pixelated with $\boldsymbol{e}^* = \boldsymbol{e}_i$ in the pixel containing the ith lattice point (see Ref. [24] for details) [32]. We find the equilibrium states at low temperatures using an MCMC method with cooling as before.

B. Results

We consider two dimensions and assume that each lattice point can take one of nine states: four ferroelectric $\mathcal{C}$ states with $s_1 = \{\boldsymbol{p}_1 = [1, 0], \boldsymbol{m}_1 = 0, \boldsymbol{e}_1 = [[1, 0], [0, -1]]\}$ and states s_2 through s_4 related to s_1 by symmetry, one zero state $s_5 = \{\boldsymbol{p}_5 = 0, \boldsymbol{m}_5 = 0, \boldsymbol{e}_5 = 0\}$, and four ferromagnetic $\mathcal{D}$ states with $s_6 = \{\boldsymbol{p}_6 = 0, \boldsymbol{m}_6 = 1/\sqrt{2}[1, -1], \boldsymbol{e}_6 = [[0, 1], [1, 0]]\}$ and states s_7 through s_9 related by symmetry. Figure 7 shows the results when $h = 2$, $J_e = J_m = D_e = D_m = D_s = 1$. Once again, we have an order-disorder phase transition, and we observe the emergence of a MPB in the form of a sharp transition at 49% from a ferromagnetic phase at low C compositions to a ferroelectric phase at high C compositions in the absence of any external fields. In particular, all ferroelectric $\mathcal{C}$ states are suppressed at low C compositions, and all ferromagnetic $\mathcal{D}$ are suppressed at high C compositions as shown in Fig. 7(a). Further, the zero state is always suppressed except at some domain walls. Thus, there are no multiferroic states except at the MPB. Furthermore, as shown in Fig. 7(b), we have classical domain walls at low and high compositions but fragmented nonclassical domain walls at the MPB.

Figure 7(c) shows the effect of external electric and magnetic fields. The application of external magnetic field leads to a ferroelectric-to-ferromagnetic phase transition while the application of an external electric field leads to

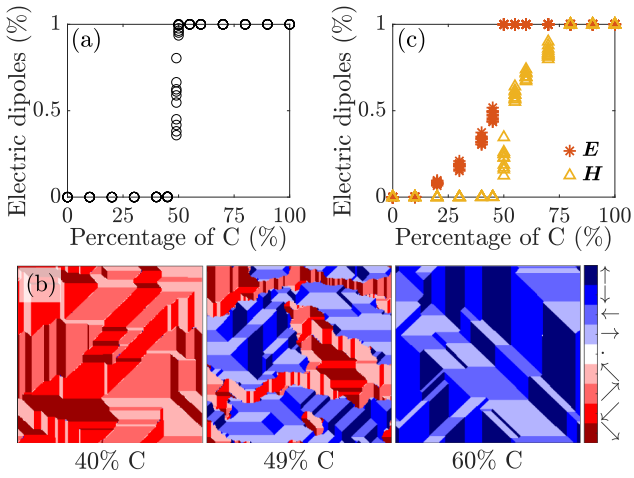

FIG. 7. Morphotropic phase boundary as means of creating a multiferroic material. (a) The ordered phase in a random lattice of a ferroelectric and ferromagnetic material shows a MPB between a ferroelectric phase and a ferromagnetic phase. (b) Domain patterns at various compositions. (c) The effect of applied field ($\boldsymbol{E} = [2\ 0]$ or $\boldsymbol{H} = [\sqrt{2}\ \sqrt{2}]$) and a ferromagnetic/ferroelectric transformation.

a ferromagnetic-to-ferroelectric phase transition at compositions close to the MPB. In other words, we have a strongly coupled multiferroic material close to the MPB. In fact recent experiments have shown the capability of chemically engineering a related type of MPB called multiferroic MPB (which is the MPB between multiferroic phases) [33,34]. Multiferroic characteristics are also found to be enhanced at the MPB of bismuth ferrite-based systems [35].

In Fig. 8, we also explore the effects of the different energy contributions in the model. Removing the strain energy (i.e., setting $D_s = 0$) does little effect in the case of the parameters used in Fig. 7. However with a stronger local field (e.g., by increasing h from 2 to 4), we find that a stronger elastic field helps to further suppress compositional disorder, leading to a sharper MPB that occurs over a narrower range of composition. This in turn results in a stronger response to external fields at the MPB and hence a more strongly coupled

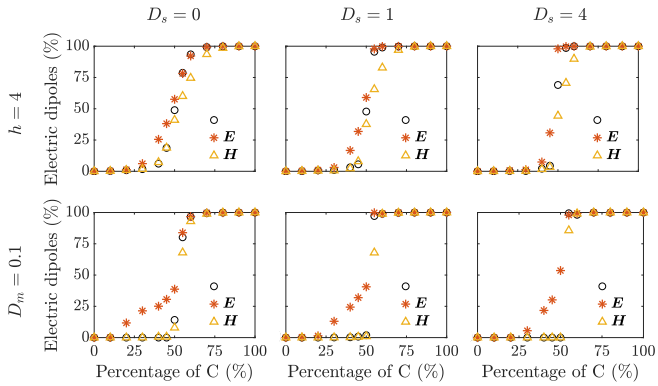

FIG. 8. The effect of local (h), magnetic (D_m), and elastic (D_s) contributions on ferromagnetic/ferroelectric transformation with and without applied field ($\boldsymbol{E} = [2\ 0]$ or $\boldsymbol{H} = [\sqrt{2}\ \sqrt{2}]$).

multiferroic system. The figure also shows the effect of reducing the magnetic contribution (D_m) relative to the electric contribution. We observe that the magnetoelectric coupling becomes asymmetric with the material being more sensitive to applied electric field compared to applied magnetic field.

All of these show that the origin of the ME coupling at the MPB is a ferroelectric-ferromagnetic phase transition. The material is ferromagnetic at low concentrations and ferroelectric at high concentrations with an exchange of stability at the MPB. The application of an electric or magnetic field changes the balance leading to the magnetoelectric coupling. Strain coupling is not necessary but can magnify the coupling.

IV. CONCLUSION

In this work, we have proposed a model based on the random field Ising model with long-range interactions motivated by perovskite solid solutions. We have used the model to study the morphotropic phase boundary, and the model provides qualitative answers to the critical open questions raised in the introduction. Specifically, the results show that both the long-range dipole-dipole interaction as well as the short-range chemical disorder are necessary for an MPB. The long-range dipole-dipole interaction overwhelms and suppresses the chemical disorder leading to a well-defined phase (crystal structure) at all compositions except the MPB. This is the reason we see distinct crystal structures away from the MPB. At the MPB, there is a change of stability from one phase to another. This balance in the other energies enables the chemical disorder to reveal itself at the MPB. This in turn leads to a frustrated and fragmented domain pattern as the disorder leads to local preference of one structure over the other. In particular, no stable and well-defined phase emerges from this disorder. Further, the disorder also leads to a number of metastable states at the MPB and these aid in domain switching and the ability to pole the material. In contrast, away from the MPB, the stable structure suppresses domain switching and the ability to pole the material.

The parameters of the model also provide various trends that can be used to tune material behavior. The paraelectric-to-ferroelectric phase transition temperature is controlled by the short-range exchange energy that manifests the balance between short-range repulsions of electron clouds and the short-range portion of the Coulomb interaction with a range of the lattice constant. Since the exchange energy depends on the average concentration, so does the transition temperature. The composition of the MPB on the other hand is controlled by the relative stability of the two phases and the relative magnitude of the polarization of the two phases. Finally, the insights gained from the model suggest a multiferroic material where the magnetoelectric coupling is a result of an MPB enabled phase transition from a ferroelectric state to a ferromagnetic state.

In short, the model is able to describe a whole range of complex phenomenology and provide qualitative answers to the questions raised in the introduction. In order to make these quantitative, it would be necessary to link the model

quantitatively to first principles calculations through multiscale modeling. This remains a task for the future. Further, we have largely studied the model through numerical simulations and mean-field arguments. It would be useful to conduct more detailed theoretical studies of the model. Finally, it would be exciting to search for multiferroic materials based on the insights here. All of these remain open issues for the future.

ACKNOWLEDGMENTS

Y.S.T. and K.B. gratefully acknowledge useful discussions with R. Bai, as well as the support of the De Logi Foundation through a gift to the California Institute of Technology (Caltech). Y.S.T. further acknowledges the support of Resnick Institute at Caltech through the Resnick Graduate Research Fellowship.

[1] K. Uchino, *Ferroelectric devices* (CRC Press, Boca Raton, Florida, 2009).
[2] R. J. D. Tilley, *Perovskites: Structure-Property Relationships* (John Wiley & Sons, Ltd, UK, 2016).
[3] E. Cross, Nature (London) **432**, 24 (2004).
[4] D. Damjanovic, J. Am. Ceram. Soc. **88**, 2663 (2005).
[5] J. Li, R. Rogan, E. Üstündag, and K. Bhattacharya, Nat. Mater. **4**, 776 (2005).
[6] J. Wu, J. Appl. Phys. **127**, 190901 (2020).
[7] B. Noheda, D. E. Cox, G. Shirane, J. A. Gonzalo, L. E. Cross, and S.-E. Park, Appl. Phys. Lett. **74**, 2059 (1999).
[8] H. Fu and R. E. Cohen, Nature (London) **403**, 281 (2000).
[9] D. Cao, I.-K. Jeong, R. H. Heffner, T. Darling, J.-K. Lee, F. Bridges, J.-S. Park, and K.-S. Hong, Phys. Rev. B **70**, 224102 (2004).
[10] D. E. Cox, B. Noheda, and G. Shirane, Phys. Rev. B **71**, 134110 (2005).
[11] N. Zhang, H. Yokota, A. M. Glazer, D. A. Keen, S. Gorfman, P. A. Thomas, W. Ren, and Z.-G. Ye, IUCrJ **5**, 73 (2018).
[12] R. Ragini, R. Ranjan, S. K. Mishra, and D. Pandey, J. Appl. Phys. **92**, 3266 (2002).
[13] S. Gorfman, D. S. Keeble, A. M. Glazer, X. Long, Y. Xie, Z.-G. Ye, S. Collins, and P. A. Thomas, Phys. Rev. B **84**, 020102(R) (2011).
[14] J. Noheda and D. E. Cox, Phase Transit. **79**, 5 (2005).
[15] I. Grinberg, V. R. Cooper, and A. M. Rappe, Nature (London) **419**, 909 (2002).
[16] I. Grinberg, V. R. Cooper, and A. M. Rappe, Phys. Rev. B **69**, 144118 (2004).
[17] D. I. Woodward, J. Knudsen, and I. M. Reaney, Phys. Rev. B **72**, 104110 (2005).
[18] R. Theissmann, L. A. Schmitt, J. Kling, R. Schierholz, K. A. Schönau, H. Fuess, M. Knapp, H. Kungl, and M. J. Hoffmann, J. Appl. Phys. **102**, 024111 (2007).
[19] L. Bellaiche, A. García, and D. Vanderbilt, Phys. Rev. Lett. **84**, 5427 (2000).
[20] Y. Wang, X. Liu, J. D. Burton, S. S. Jaswal, and E. Y. Tsymbal, Phys. Rev. Lett. **109**, 247601 (2012).
[21] P. P. Ewald, Ann. Phys. **369**, 253 (1921).
[22] J. J. Cerdà, V. Ballenegger, O. Lenz, and C. Holm, J. Chem. Phys. **129**, 234104 (2008).
[23] D. Wang, J. Liu, J. Zhang, S. Raza, X. Chen, and C.-L. Jia, Comp. Mater. Sci. **162**, 314 (2019).
[24] See Supplemental Material at http://link.aps.org/supplemental/10.1103/PhysRevB.103.144201 for derivations and plots.
[25] Y. C. Shu and K. Bhattacharya, Phil. Mag. B **81**, 2021 (2001).
[26] M. Aizenman and J. Wehr, Phys. Rev. Lett. **62**, 2503 (1989).
[27] T. Nattermann, in *Spin Glasses and Random Fields*, edited by A. P. Young (World Scientific, Singapore, 1997), pp. 277–298.
[28] L. C. Sampaio, M. P. De Albuquerque, and F. S. de Menezes, Phys. Rev. B **54**, 6465 (1996).
[29] V. Kovacova, N. Vaxelaire, G. Le Rhun, P. Gergaud, T. Schmitz-Kempen, and E. Defay, Phys. Rev. B **90**, 140101(R) (2014).
[30] A. K. Kundu, *Magnetic Perovskites* (Springer, India, 2016).
[31] N. A. Hill, J. Phys. Chem. B **104**, 6694 (2000).
[32] R. Bai, Y. S. Teh, and K. Bhattacharya, Extreme Mech. Lett. **43**, 101160 (2021).
[33] J. Zhuang, L.-W. Su, H. Wu, A. A. Bokov, M. Liu, W. Ren, and Z.-G. Ye, Appl. Phys. Lett. **107**, 182906 (2015).
[34] J. Zhuang, J. Lu, N. Zhang, J. Zhang, A. A. Bokov, S. Yang, W. Ren, and Z.-G. Ye, J. Appl. Phys. **125**, 044102 (2019).
[35] Y. N. Zhou, T. T. Gao, J. Chen, X. Q. Liu, and X. M. Chen, J. Alloys Compd. **819**, 153031 (2020).